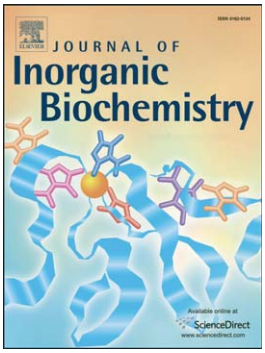

Enhancing the copper(II) complexes cytotoxicity to cancer cells through bound to human serum albumin

Yi Gou, Yao Zhang, Jinxu Qi, Zuping Zhou, Feng Yang, Hong Liang

PII: S0162-0134(14)00305-5
DOI: doi: 10.1016/j.jinorgbio.2014.12.012
Reference: JIB 9635

To appear in: *Journal of Inorganic Biochemistry*

Received date: 19 August 2014
Revised date: 10 December 2014
Accepted date: 10 December 2014

Please cite this article as: Yi Gou, Yao Zhang, Jinxu Qi, Zuping Zhou, Feng Yang, Hong Liang, Enhancing the copper(II) complexes cytotoxicity to cancer cells through bound to human serum albumin, *Journal of Inorganic Biochemistry* (2014), doi: 10.1016/j.jinorgbio.2014.12.012

Enhancing the copper(II) complexes cytotoxicity to cancer cells through bound to human serum albumin

Yi Gou, Yao Zhang, Jinxu Qi, Zuping Zhou, Feng Yang*, Hong Liang*

State Key Laboratory Cultivation Base for the Chemistry and Molecular Engineering of Medicinal Resources, Ministry of Science and Technology of China, Guangxi Normal University, Guilin, Guangxi, China

*Corresponding authors: (F. Yang) E-mail: jxyangfeng@gmail.com; (H. Liang) E-mail: hliang@mailbox.gxnu.edu.cn; Phone/Fax: 86-773-212-0958; Postal address: 15 Yucai Road, Guilin, Guangxi, China. Zip code: 541004

Abstract

We use Schiff-base salicylaldehyde benzoylhydrazone (**HL**) as the ligand for Copper(II), resulting in the complexes $[CuCl(L)]\cdot H_2O$ (**C1**), $[CuNO_3(L)]\cdot H_2O$ (**C2**) and $[CuBr(L)]_2$ (**C3**). We characterize the Cu(II) compounds' interactions with human serum albumin (HSA) using fluorescence spectroscopy and molecular docking. These studies revealed that Cu(II) compounds propensity bound to IIA subdomain of HSA possible by hydrophobic interactions and hydrogen bond. Cu(II) compounds produce intracellular reactive oxygen species (ROS) in cancer cells. Complexes of HSA and copper(II) compounds enhance about 2-fold cytotoxicity in cancer cells but do not raise cytotoxicity levels in normal cells *in vitro*. Compared with **C3** alone, HSA–**C3** complex promotes HepG2 cell apoptosis and has a stronger capacity to promote cell cycle arrest at the G2/M phase of HepG2.

Keywords: copper(II) compound; human serum albumin; cytotoxicity; cell apoptosis

1. Introduction

In the 1950s, salicylaldehyde benzoylhydrazone (**HL**) was found to possess mild bacteriostatic activity when tested *in vitro* against microorganisms such as *Mycobacterium tuberculosis*, *Candida albicans* and *Mycobacterium smegmatis* [1]. It was noted that **HL**, in particular, appeared to be an unusually potent inhibitor of DNA synthesis and cell growth in a variety of human and rodent cell lines grown in culture [2−4]. Subsequently, a range of tridentate ONO hydrazones, including **HL**, were evaluated as iron-chelating drugs *in vivo* and **HL** was found to mobilize iron from iron-loaded reticulocytes *in vitro* [5, 6]. Interestingly, copper(II) complexes showed significantly stronger anticancer activity than did free ligands [7]. Due to biological interest in copper chelate systems, a number of single-crystal x-ray structural studies have been carried out on copper with **HL** and its analogues [8−12]. Unfortunately, their poor water solubility and moderate anti-proliferative characteristics have hindered their potential for application and, therefore, little is known about the bioactivity mechanisms of these compounds [8, 13].

A promising approach to circumvent the poor water solubility of metal compounds and to improve their efficacy towards malignant cells is to couple anticancer drugs to suitable carrier macromolecules. Various types of macromolecules have been used as carrier molecules, including

poly (ethylene glycol) polymers, nanoparticles, nanotubes, liposomes, dendrimers and protein biomolecules [14, 15]. Among them, human serum albumin (HSA) is promising for drug carrier owing to its unique biochemical and pharmacological characteristics [16−18]. Current studies showed that HSA not only increases the solubility of metal compounds, but also enhances their antitumour activity [19−24]. HSA is the most abundant protein in blood plasma, which plays a central role in drug pharmacokinetics and distribution [25]. In order to better develop drugs, it is necessary to understand the interactions of lead drugs and HSA [26, 27]. To date, the interactions of HSA with metal compounds have been extensively investigated [28]. The studies revealed that the modes of metal compounds interacting with HSA are interesting. For example, the axial maleimide of a Pt(IV) complex forms a covalent bond with the sole free cysteine thiol of HSA [29]. The ruthenium compounds could bind to HSA either through direct coordination to HSA or in a non-coordinate fashion [19, 20, 30]. Meanwhile, many copper anticancer compounds have also been synthesized and studied on their interactions with HSA [31−36].

With this background in mind and considering that copper is a crucial trace element in redox chemistry specific to the growth and development in all living organisms [37], we attempted to synthesize copper(II) compounds by reacting $CuCl_2$/$Cu(NO_3)_2$/$CuBr_2$ with **HL** in methanol. We

were excited to obtain a novel phenolic oxygen-bridged binuclear copper(II) compound **C3** (Scheme 1). It is worth mentioning here that many metalloenzymes and proteins contain in their active sites two copper ions that operate cooperatively [38–41]. Thus, a great deal of attention has been given to bimetallic copper compounds with two metal ions in close proximity because they provide an opportunity to study intramolecular binding, bimetallic catalysts, magnetic exchange interactions, multi-electron redox reactions and an activity mimicking the possible activation of small substrate molecules by enzymes [42–45]. While there have been a few reports about **C1** and **C2** in the literature, no attempt has been made to explore the effect of compounds binding to HSA [46–48]. In this study, we tested the antiproliferative activity of **HL** and **C1**–**C3** compounds in the human cancer cell line. Our results indicate that these copper(II) compounds bound with HSA can improve their bioactivity.

2. Experimental section

2.1 Material

HSA (fatty acid content < 0.05%) was purchased from the Sigma Chemical Company and used without further purification. All other chemicals and solvents used were of high purity and available from commercial sources. Water used in the reactions was distilled prior to use.

Elemental analyses (C, N, and H) were carried out on a Perkin-Elmer 2400 analyzer. Infrared (IR) spectra were recorded using KBr pellets (4000–400 cm^{-1}) on a Nexus 870 FT-IR spectrophotometer. UV–visible spectra were measured on a Cary 1E UV-Visible spectrophotometer in the 200–800 nm range.

2.2. Synthesis of copper compounds

Compounds **HL**, **C1** and **C2** were synthesized according to literature procedures [46–48].

*2.2.1. Synthesis of $[CuBr(L)]_2$ (**C3**)*

Benzoylhydrazine (0.27 g, 2 mmol) and salicylaldehyde (0.24 g, 2 mmol) were dissolved in an aqueous methanol solution (15 mL) and stirred 1 h to give an orange solution, which was added to a methanol solution (15 mL) of $CuBr_2$ (0.44 g, 2 mmol). The mixture was stirred for another 30 min at room temperature to give a celadon solution and then filtered. The filtrate was kept in air for a week, forming blue block crystals. The crystals were isolated, washed three times with distilled water and dried in a vacuum desiccator containing anhydrous $CaCl_2$. Yield: 616 mg (65%). *Anal*. Calcd for $C_{28}H_{22}Br_2Cu_2N_4O_4$ (765.40): C, 43.94; H, 2.89 and N, 7.32. Found: C, 43.95; H, 2.89 and N, 7.33. IR (KBr, cm^{-1}): 1600 ν(C=N); 555, 511, 476, 446 ν(Cu–N/Cu–O) .

2.3. Crystal structure determinations

X-ray crystallographic data were collected on a Bruker SMART Apex II CCD diffractometer using graphite-monochromated Mo-Kα (λ = 0.71073 Å) radiation. Empirical adsorption corrections were applied to all data using SADABS. The structures were solved by direct methods and refined against F^2 by full-matrix least-squares methods using the SHELXTL version 5.1 [49]. All of the non-hydrogen atoms were refined anisotropically. All other hydrogen atoms were placed in geometrically ideal positions and constrained to ride on their parent atoms. The crystallographic data for compound **C3** are summarized in Table 1. Selected bond lengths and angles are given in Table 2.

2.4. Density functional theory (DFT) calculations

All of the calculations were done with the GAMESS suite of codes [50]. The DFT/B3LYP [51, 52] method was used for the electronic structure determination. Considering both the calculation cost and the accuracy, we used the 6-311+G with a set of ‘‘d’’ and ‘‘p’’ polarization functions for Cu and Br and 6-31+G(d,p) for the rest atoms. The contribution of a group to a molecular orbital was calculated using Mulliken population analysis. *GAUSSSUM 2.2* [53] was used to calculate group contributions to the molecular orbitals. A natural bond orbital

(NBO) analysis was also made for **C3** using the NBO code [54]. A detailed topological analysis of the electron density was made according to atoms in molecules (AIM) theory, using the program Multiwfn [55]. The atomic coordinates were obtained from the x-ray structures.

2.5. Biology

2.5.1. Cell culture

Culture medium DMEM (with L-glutamin), Fetal bovine serum (FBS), PBS (phosphate buffered saline) (pH = 7.2) and Antibiotice-Antimycotic were from E.U Gibco BRL. Human cervical cancer cell lines HeLa, human lung carcinoma cell lines A549, human liver hepatocellular carcinoma cell lines HepG2 and human liver cell lines HL-7702 (purchased from the American Type Culture Collection and the German Collection of Microorganisms and Cell Cultures) were maintained in DMEM supplemented with 10% FBS, 50 U/mL penicillin, 50 mg/mL streptomycin at 37 °C and 5% CO_2.

2.5.2. 3-(4,5-Dimethylthiazol-2-yl)-2,5-diphenyltetrazolium bromide (MTT) cytotoxicity assay

To gain deeper insight into the effect of HSA interactions on the activity of the compounds, two sets of experiments were performed: (1)

all compounds were dissolved in PBS with 0.5% DMSO and incubated with HSA for 24 h at room temperature, after which the HSA–complexes incubated with above human cancer cell lines for 48 h, and (2) all compounds were dissolved in PBS with 0.5% DMSO and then tested. The MTT assay was performed according to the literature method [56]. Briefly, 100 μL of cell suspensions at a density of 5×10^4 cells/mL was seeded in triplicate in 96-well plates and incubated for 24 h at 37 °C in 5% CO_2. Then the medium was replaced with the respective medium with 10% FBS containing the compounds at various concentrations and incubated at 37 °C under conditions of 5% CO_2 for 48 h. The final DMSO concentration in all experiments was < 0.5% in medium. The absorbance of the converted dye in living cells was measured at a wavelength of 570 nm. Values shown are the mean values of at least three measurements. IC_{50} values (the drug concentrations that reduced the number of viable cells to 50% of the control level) were determined by the nonlinear multipurpose curve-fitting program GraphPad Prism.

2.5.3. Apoptosis by Flow Cytometry

The apoptotic events induced by the copper(II) compound (**C3**) and HSA–copper(II) complex (HSA–**C3**) were determined by annexin V staining and PI according to the manufacturer's protocol for the Annexin V-FITC Apoptosis Detection Kit (Abcam). For these analyses, we used 1

× 10^5 cells/mL, which were incubated at 5% CO_2 and 37 °C with the **C3** and HSA–**C3** for 12 h. The HepG2 cells were resuspended in 100 μL 1 × annexin V-binding buffer (10 mM Hepes/NaOH, 140 mM NaCl, 2.5 mM $CaCl_2$, pH 7.4), and 5 μL each of annexin V and PI were added to each sample. Next, we incubated the cells for 15 min at room temperature and then subjected them to flow cytometric analysis (FACScan, Bection Dickinson, San Jose, CA). The rate of cell apoptosis was analyzed.

2.5.4. Cell cycle distribution analysis

HepG2 cells were cultured in 70-mm culture dishes, grown to 70% confluence, and treated with concentration of **C3** and HSA–**C3** determined by their IC_{50} values. FACS analysis was performed after 24 h of treatment as described [57]. For cell cycle analysis, the washed cells were fixed with 75% ethanol, washed with PBS, stained with PI and analyzed by flow cytometry using a 488 nm laser (FACScan, Bection Dickinson, San Jose, CA). For each sample, 10000 events were recorded.

2.5.5. Intracellular reactive oxygen species (ROS) Measurements

Intracellular ROS generation was determined using 2',7'-dichlorodihydro-fluorescein diacetate (H_2DCF-DA) [58] (Beyotime Institute of Biotechnology, Haimen, China). HepG2 cells (1 × 10^5 cells/well) were incubated with either **HL** (0.25 μM), Cu(II) (0.25 μM),

C1–**C3** (0.25 μM) or their HSA–complexes (0.25 μM) for 48 h at 37 °C. Cells were collected for flow cytometric assessment. The fluorescence intensity was monitored with excitation wavelength at 488 nm and emission wavelength at 525 nm.

2.5.6. Statistical Analysis

All experiments were repeated 3 to 5 times. Student's *t* test was applied to evaluate the significance of differences measured. Results were expressed as mean ± SD and considered to be significant when $p < 0.05$.

2.6. Protein binding studies

Protein-binding studies were performed by fluorescence quenching experiments using HSA. HSA solution (1 μM) was titrated by successive additions of test solutions **C1**–**C3** using micropipettes for all of the experiments. The fluorescence emission spectra were scanned from 300 to 420 nm after excitation at 280 nm (the maximum emission was obtained at 347). The binding constant of HSA for compounds can be analyzed according to the Scatchard equation [59]:

$$\log[(F_0 - F)/F] = \log K + n \times \log(Q) \quad (1)$$

where F and F_0 are the fluorescence intensities of protein in the presence and absence of the quencher, respectively; n is the number of binding sites; K is the binding constant and [Q] is quencher concentration. From

the plot of log[(F_0—F)/F] versus log [Q], the number of binding sites (n) and the binding constant (K) was calculated.

The fluorescence quenching mechanism was usually analyzed using the well-known Stern–Volmer equation [60]:

$$F_0/F = 1 + K_q \tau_0 [Q] \quad (2)$$

where K_q is the quenching rate constant of the biological macromolecule, τ_0 is the average lifetime of the protein without any quencher and the fluorescence lifetime of the biopolymer is 10^{-8} s [61].

Thermodynamic parameters were calculated based on the temperature dependence of the binding constant for compounds–HSA binding. The temperatures used were 298, 310 and 320 K. The enthalpy change (ΔH^0) was calculated from the slope of the Van't Hoff equation [62]:

$$\ln K = -\Delta H^0/RT + \Delta S^0/R \quad (3)$$

The value of ΔS^0 was also obtained from the linear Van't Hoff plot. The free energy changes (ΔG^0) at different temperatures (T) can be calculated from the following relationship:

$$\Delta G^0 = \Delta H^0 - T\Delta S^0 \quad (4)$$

In Eq. (3) and (4), R is gas constant and K is the binding constant at temperature T. Owing to the temperature only changes a little, the enthalpy change (ΔH^0) can be regarded as a constant.

2.7. Molecular modeling

AutoDock 4.2 (graphical user interface) [63] was used for protein–ligand docking and the crystal structure of HSA was retrieved from the Protein Data Bank (PDB code: 1BJ5). All the water molecules and the bound ligands were removed prior to modeling experiments. Preparation of the 1BJ5 protein with AutoDock Tools (ADT) involved the addition of polar hydrogen atoms, partial charge correction and finally, Gasteiger charges were calculated for each atom of the protein. Affinity grid maps of 40 × 45 × 40 Å grid points and 0.375 Å spacing were generated using AutoGrid program. Docking calculations consisted of 2.5×10^7 energy evaluations using the Lamarckian genetic algorithm (LGA) method. The obtained 100 docked structures were clustered according to 2.0 Å RMSD (root-mean-square deviation) and were arranged according to their binding energies and population criteria for each analysis as well as the main interactions between the copper(II) compounds and the binding site of the receptor.

3. Results and Discussion

3.1. Crystal structure description

The compound **C3** crystallizes in the triclinic system, space group *P*-1. It contains two Schiff-base ligands, two Cu atoms and two Br (Fig 1A). Phenolic oxygen atoms from a neighbouring molecule act as bridging

atoms to the phenolato-bridged dinuclear copper(II) centre, with a typical Cu···Cu distance of about 3.026 Å. The centroid of the **C3** dimer lies on an inversion centre i.e. the second part of the dimer is generated by symmetry. Both Cu atoms (Cu1 and Cu1^{i}, symmetry code: (i) 1 − *x*, − *y*, 2 − *z*) are five-coordinated by three oxygen atoms from two different Schiff-base ligands, a nitrogen atom from a Schiff base-ligand and one terminal Br atom. The coordination geometry in this compound is very similar to that in $[CuCl(L1)]_2$ [12]; the only difference is the presence of a Cl atom at the apical position. All Cu−X bond distances are very similar to those reported in related copper(II) hydrazone compounds [12, 46–48]. The coordination polyhedron around the Cu1 centre could be described as a slightly-distorted square pyramid (τ = 0.11) [64], with the metal displaced from the O1/O2^{i}/N1/O2 basal plane (maximum displacement 0.08 Å for the N1 atom), and the Br2 atom at the apex, with the metal displaced by 0.299 Å toward Br2 from the mean basal plane. In the solid state, the discrete copper(II) dimers of **C3** were further linked into a one-dimensional (1D) polymeric chain by the N–H···Br interactions involving a nitrogen atom (N2) from a Schiff-base ligand and a bromine atom (Br2^{ii}) bonded to the Cu1^{ii} (N2···Br2^{ii} = 3.29 Å and the N2–H1N···Br2^{ii} angle is 173.2^{o}, symmetry code: (ii) –1 + *x*, *y*, *z*, Fig 1B). Interestingly, there is a $\pi\cdots\pi$ stacking arising from the aromatic rings of the Schiff-base ligands in the layers, as shown in Fig 1C (face-to-face distance: 3.35 Å and

centre-to-centre distance: 4.04 Å) [65]. In this study, the resulting structure of the dimeric **C3** copper(II) compound displayed a 2D 4-connected net with sql ($4^4.6^2$) topology as shown in Fig 1D.

3.2. Theoretical calculations

To gain insight into **C3**'s electronic structures and bonding properties, we used the density functional theory (DFT) method for our calculations. The formal charge of copper is + 2 in **C3**. However, the calculated charge on the copper atom, obtained from natural population analysis, is approximately 0.98 in **C3**. The charge on the Br ligands is equal to –0.72 and those on the O1, O2 and N1 are –0.63,–0.75 and –0.32, respectively. This is a result of charge donation from the ligands to the copper centre. The natural atomic orbital *d* occupancies are as follows: d_{xy} 1.544, d_{xz} 1.982, d_{yz} 1.984, d_{x2-y2} 1.758 and d_{z2} 1.975 in **C3**. These data suggest that the donation from the ligands to the d_{Cu} orbitals plays a key role in **C3**'s electronic structure. In the frontier region, the highest occupied molecular orbital (HOMO) and the HOMO–1 of **C3** are localized on copper atoms characterized by a significant contribution from Br ligands. The frontier molecular orbitals of **C3** are depicted in Fig. S1. The lowest unoccupied molecular orbital (LUMO) is located on copper (75% β spin) with an admixture of Schiff-base ligands (99% α spin). Similarly the LUMO+1 is

primarily localized on copper (47% β spin) with an admixture of the Schiff-base ligands (98% α spin).

In this study, we applied the quantum theory of atoms in molecules (QTAIM) to analyse the strength of the metal–ligand interaction. Table 3 lists the (3, −1) bond critical points (BCPs) and (3, +1) ring critical points (RCPs) of the charge density, and the BCP electron densities (ρ_{BCP}) results indicate that the Cu–halogen bonds are weaker than the Cu–N/Cu–O bonds. In **C3**, an electron charge density ρ_{BCP} bond order of Cu1–N1 < Cu1–O2 < Cu–O1 < Cu–O2^{i} is seen at the critical point of the Cu–N/O bonds, which is in consistent with the inversely proportional decrease in bond lengths from Cu1–N1 to Cu1–O2^{i}. All BCPs are characterized by ρ_{BCP} and $\nabla^2\rho_{BCP}$ values in keeping with shared (C–O, C–N, C=N and C–H bonds) and closed shell (Cu–O, Cu–N and Cu–Br bonds) behaviours. The positive $\nabla^2\rho_{BCP}$, negative H_{BCP} and the G_{BCP}/V_{BCP} ratio all indicate that the Cu–O, Cu–N and Cu–Br bonds belonged to partially covalent interactions. The ellipticity ε, defined as $\varepsilon = \lambda_1/\lambda_2 – 1$, is a measure of the ratio of the rate of density decrease in the two directions perpendicular to the bond path at the BCP, the degree of π-character and the general shape of the bond. This value is zero for the standard single/triple bond because the electron density distribution at this BCP is symmetric. The ε values of all Cu–N, Cu–O and Cu–Br bonds are nonzero. This is attributable to the

preferential accumulation in the direction parallel to the N/O/Br lone pair. Interestingly, we found two additional intermolecular hydrogen bonds, C13–H13···O1^{i} and C13i–H13^{i}···O1 (Fig 2 and S2). In Table 3 we report the geometrical properties and topological parameters associated with these hydrogen bonds. According to a hydrogen bond classification based on geometrical parameters [66], their features (C···O = 3.05 Å, H···O = 2.26 Å and a C–H···O angle of 141.6º) correspond with those of moderate hydrogen bonds, which also have relatively low interaction energies (E_{HB} = 13.01 kJ·mol^{-1} [67]).

3.3. Anticancer properties of copper(II) compounds and HSA-C3 complex

The results in Table 4 indicate that Cu(II) and HL show relatively low activity against the cancer cells, but the **C1**–**C3** compounds show high cytotoxicity against cancer cells. This implies that the chelation of the Cu(II) ion with **HL** is responsible for the observed high cytotoxic properties of the **C1**–**C3** compounds. Specifically, **C3** has higher cytotoxicity than either **C1** or **C2**. While HSA can improve the efficiency of anticancer agents such as chlorambucil, doxorubicin and some Ru-based and Pt-based compounds [19, 20, 68–71], the next question is whether or not HSA can influence the anticancer activity of Cu(II) compounds? To answer this question, we performed MTT assays to

evaluate its performance *in vitro*. It should be noted that in general, the pre-incubation of copper(II) compounds with HSA has resulted in increased activity in the mortality of cancer cell lines, while leaving normal cells (HL-7702) no improving. HSA, by itself, has no cytotoxic effect on cancer cells or normal cells (Table 4).

Does HSA affect the apoptosis and cell cycle arrest induced by Cu(II) compounds? To investigate this question, we first looked at **C3** and HepG2 cells because the HSA–**C3** complex has high cytotoxic activity in HepG2 cells relative to other cancer cell lines. Results from Annexin V-FITC/PI staining showed that the percentage of apoptosis in HepG2 cells is 9.87% for **C3** and 27.9% for HSA–**C3**, indicating that HSA–**C3** can promote apoptosis in cancer cells (Fig 3). Furthermore, the percentage of cell numbers in the G2/M phase treated with **C3** was 15.42%, but this percentage increased to 28.69% when the G2/M phase was treated with HSA–**C3**. In contrast, the percentage of untreated control cells in the G2/M phase was 7.04% (Table 5). These results suggest that **C3** may cause an accumulation of cells in the G2/M phase of the cell cycle by delaying or inhibiting cell cycle progression at the G2/M phase. Clearly, HSA improves the **C3**'s capacity for cell cycle accumulation at the G2/M phase. In addition, we found that the effects of **C3** on cell cycle distribution patterns were dose-dependent, as shown in Fig 4. According

to our results, HSA has a significant influence on **C3** anticancer properties, improving its efficiency to a certain extent. The most likely reason is that the complexes are more soluble when bound to HSA, which results in (slightly) more toxicity over the 48 h period that they used.

3.4. Intracellular ROS Assay

Reactive oxygen species (ROS), including O_2^-, H_2O_2 and HO^-, are generated during aerobic metabolism. ROS play an important role in cell signalling and homeostasis [72, 73]. Cancer cells exhibit greater ROS stress than do normal cells. A cancer cell can die in one of three ways: apoptosis, necrosis and autophagy. At low levels, ROS facilitate cancer cell survival and proliferation [74, 75]. But excessive levels of ROS can result in apoptosis, autophagy and necrosis in cancer cells [76, 77].

Previous results have demonstrated that copper-based compounds can produce intracellular ROS in SK-N-MC cells [58]. Do cancer cells produce intracellular ROS when induced by **C1**–**C3** compounds? To answer this question, we examined the ability of these compounds to catalyse the production of intracellular ROS in HepG2 cells by using a fluorescent 2',7'-dichlorofluorescein (DCF) probe and flow cytometry. The results showed that the incubation of HepG2 cells with **C1**–**C3** and their HSA complexes led to a shift of the DCF fluorescence peak to the

right, relative to that of the control cells (Figs 5A–C), reflecting increased oxidative damage to these cell populations by the Cu(II) compounds. We quantified the DCF fluorescence peaks of these compounds and the results are shown in Fig 5D. These results demonstrate that **C3** caused a significant ($p < 0.01$) increase in 2',7'-dichlorodihydrofluorescein (H_2DCF) oxidation to 547 ± 18% in the control cells after 48 hours incubation. The **C3** was found to be 57% and 53% more effective than **C1** and **C2**, respectively, in inducing intracellular ROS. Importantly, the high redox activity, 0.25 μM, of the HSA–**C3** complex was significantly ($p < 0.01$) greater (785 ± 31%) than the 0.25 μM activity of the **C3** after 48 hours. Similar results were found for **C1** and **C2** (Fig 5). Hence, the enhanced permeability of the Cu(II) compounds due to the presence of HSA as a carrier likely plays an important role in the increased intracellular redox activity observed. However, no significant increase in H_2DCF oxidation was observed with the same concentrations of **HL**, HSA–**HL** and Cu(II) alone over this same incubation period. These results suggest that these compounds' marked antitumor activity may due to their ability to generate cytotoxic ROS during a redox cycle [70].

3.5. Binding properties of three compounds to HSA

HSA may increase the solubility of metal compounds [19]. To test this idea, we added **C1**–**C3** compounds to an HSA solution and incubated the mixtures for 3 hours in the dark at room temperature. The resultant dispersion was centrifuged for 10 min at 4000*g* to remove the precipitates. As shown in Fig 6, the UV intensity of the supernatant was significantly higher (6-fold for **C1**, 5.2-fold for **C2** and 3-fold for **C3**) than that of the identically treated **C1**–**C3** solutions without HSA. This suggests that the solubility of copper compounds may be changed by their binding with HSA. Therefore, to better understand how copper compounds bind with HSA, we investigated the binding properties of Cu(II) compounds with respect to HSA using fluorescence spectroscopy and molecular docking.

The fluorescence of HSA at around 347 nm was gradually quenched upon increasing the concentration of compounds **C1**–**C3** with a little blue shift (*ca.* 3 nm, 4 nm and 2 nm for **C1**, **C2** and **C3**, respectively) (Fig 7A and S3). These data indicated that copper(II) compounds interact with HSA and quench its intrinsic fluorescence. We calculated the HSA quenching rate constants (K_q) [Eq. (2)] to be 1.19 (± 0.02) × 10^{14} M^{-1} s^{-1} for **C1**, 1.37 (± 0.03) × 10^{14} M^{-1} s^{-1} for **C2** and 1.87 (± 0.05) × 10^{14} M^{-1} s^{-1} for **C3** at 298 K (Fig 7B). The calculated K_q values are much larger than the maximum scattering collision quenching constant (2.0 × 10^{10} M^{-1} s^{-1}), which implies that the fluorescence quenching of HSA is initiated by the formation of the HSA and **C1**–**C3** complexes rather than

by dynamic collision. The binding constant *K* is calculated according to Eq. (1) (Fig 7C). The *K* values of HSA for **C1**–**C3** were found to be 0.41 (± 0.04) × 10^5 M^{-1}, 1.51 (± 0.03) × 10^5 M^{-1} and 7.94 (± 0.07) × 10^5 M^{-1} at 298 K, respectively. The value of n (0.89 for **C1**, 0.91 for **C2** and 1.01 for **C3**) indicates the existence of a single binding site in HSA for these compounds (Table 6).

Meanwhile, we calculated the thermodynamic parameters for **C1**–**C3** binding to HSA using Eqs. (3) and (4), and these parameters are presented in Table 6. The binding process is spontaneous because $\Delta G^0 <$ 0. A comparison of the binding affinity of **C1**–**C3** for HSA at different temperatures (298, 310 and 320 K) clearly shows that **C3** has a relatively low ΔG^0 (*ca.* −34 kJ·mol^{-1}) for HSA. That $\Delta H^0 < 0$ and $\Delta S^0 > 0$ reveals that **C1**–**C3** interact with HSA mainly by hydrophobic interactions and hydrogen bonds [62].

We carried out molecular modelling using AutoDock software to build possible mode of the interaction of copper(II) compounds and HSA. The docking results reveal that Cu compounds are located within the binding pocket of IIA subdomain of HSA (Fig 8). This region consists of a modestly flexible hydrophobic cavity delimited by some polar and hydrophobic residues. Besides hydrophobic interactions, Cu complexes form possible hydrogen bond with polar residue (Fig 8).

4. Conclusion

Since the chelation of copper(II) ion with a ligand results in a synergistic effect, Cu(II) compounds derived from salicylaldehyde benzoylhydrazone possess high anticancer activities. Furthermore, the binuclear Cu(II) compound (**C3**) shows stronger anticancer activity than mononuclear copper compounds (**C1** and **C2**). The efficiency of copper(II) compounds can be enhanced to some extent by their binding with HSA. Our results may be helpful in the development of copper(II) hydrazone compounds for lead drug applications.

Acknowledgements

This work was supported by the Natural Science Foundation of China (31060121, 31460232, 21171043 and 21431001), Natural Science Foundation of Guangxi (2012GXNSFCB053001, 2013GXNSFGA019010 and 2014GXNSFDA118016), Technology division of Guilin (20130403-1) and Guangxi 'Bagui' scholar program to ZF Chen and ZP Zhou.

References

[1] H.A. Offe, W. Siefken, G. Domagk, Z. für Naturforsch. B 7 (1952) 446–462.

[2] D.K. Johnson, T.B. Murphy, N.J. Rose, W.H. Goodwin, L. Pickart, Inorg. Chim. Acta 67 (1982) 159–165.

[3] L. Pickart, W.H. Goodwin, W. Burgua, T.B. Murphy, D.K. Johnson, Biochem. Pharmacol. 32 (1983) 3868–3871.

[4] L.M. Wu, H.B. Teng, X.C. Feng, X.B. Ke, Q.F. Zhu, J.T. Su, W.J. Xu, X.M. Hu, Cryst. Growth Des. 7 (2007) 1337–1342.

[5] P. Ponka, J. Borová, J. Neuwirt, O. Fuchs, E. Necas, Biochim. Biophys. Acta 586 (1979) 278–297.

[6] D.K. Johnson, M.J. Pippard, T.B. Murphy, N.J. Rose, J. Pharmacol. Exp. Ther. 221 (1982) 399–403.

[7] H.H. Monfared, M.V. ahedpour, M.M. Yeganeh, M. Ghorbanloo, P. Mayer, C. Janiak, Dalton Trans. 40 (2011) 1286–1294.

[8] J.D. Ranford, J.J. Vittal, Y.M. Wang, Inorg. Chem. 37 (1998) 1226–1231.

[9] E.W. Ainscough, A.M. Brodie, A. Dobbs, J.D. Ranford, J.M. Waters, Inorg. Chim. Acta 236 (1995) 83–88.

[10] S.C. Chan, L.L. Koh, P.-H. Leung, J.D. Ranford, K.Y. Sim, Inorg. Chim. Acta 236 (1995) 101–108.

[11] E.W. Ainscough, A.M. Brodie, A. Dobbs, J.D. Ranford, J.M. Waters, Inorg. Chim. Acta 267 (1998) 27–38.

[12] M. Alagesan, N.S.P. Bhuvanesh, N. Dharmaraj, Eur. J. Med. Chem. 78 (2014) 281–293.

[13] E.W. Ainscough, A. M. Brodie, W.A. Denny, G. J. Finlay, S.A. Gothec, J.D. Ranford, J. Inorg. Biochem. 77 (1999) 125–133.

[14] R. Haag, F. Kratz, Angew. Chem. Int. Ed. 45 (2006) 1198–1215.

[15] S.E.A. Gratton, P.A. Ropp, P.D. Pohlhaus, J. Christopher Luft, V.J. Madden, M.E. Napier, J.M. DeSimone, P. Natl. Acad. Sci. USA 105 (2008) 11613–11618.

[16] F. Kratz, J. Control. Release 132 (2008) 171–183.

[17] F. Kratz, J. Control. Release 190 (2014) 331–336.

[18] F. Kratz, Bakheet Elsadek, J.Control. Release 161 (2012) 429–445.

[19] M.I. Webb, B.Wu, T. Jang, R.A. Chard, E.W.Y. Wong, M.Q. Wong, D.T.T. Yapp, C.J. Walsby, Chem. Eur. J. 19 (2013) 17031–17042.

[20] I.N. Stepanenko, A. Casini , F. Edafe, M.S. Novak, V.B. Arion, P.J. Dyson, M.A. Jakupec, B.K. Keppler, Inorg. Chem. 50 (2011) 12669−12679.

[21] W.H. Ang, E. Daldini, L. Juillerat-Jeanneret, P.J. Dyson, Inorg. Chem. 46 (2007) 9048−9050.

[22] Y.R. Zheng, K. Suntharalingam, T.C. Johnstone, H. Yoo, W. Lin, J.G. Brooks, S.J. Lippard, J. Am. Chem. Soc. 136 (2014) 8790−8798.

[23] A. Warnecke, I. Fichtner, D. Garmann, U. Jaehde, F. Kratz, Bioconjugate Chem. 15 (2004) 1349–1359.

[24] B.T. Benedetti, E.J. Peterson, P. Kabolizadeh, A. Martínez, R. Kipping, N.P. Farrell, Mol. Pharmaceut. 8 (2011) 940–948.

[25] T. Peters, All about albumin: biochemistry, genetics and medical applications, Academic Press, San Diego (1995).

[26] T. Oltersdorf, S.W. Elmore, A.R. Shoemaker, R.C. Armstrong, D.J. Augeri, B.A. Belli, M. Bruncko, T.L. Deckwerth, J. Dinges, P.J. Hajduk, M.K. Joseph, S. Kitada, S.J. Korsmeyer, A.R. Kunzer, A. Letai, C. Li, M.J. Mitten, D.G. Nettesheim, S. Ng, P.M. Nimmer, J.M. O'Connor, A. Oleksijew, A.M. Petros, J.C. Reed, W. Shen, S.K. Tahir, C.B. Thompson, K.J. Tomaselli, B. Wang, M.D. Wendt, H. Zhang, S.W. Fesik, S.H. Rosenberg, Nature 435 (2005) 677–681.

[27] T. Vallianatou, G. Lambrinidis, A. Tsantili-Kakoulidou, Expert Opin. Drug Dis. 8 (2013) 583–595.

[28] A.R. Timerbaev, C.G. Hartinger, S.S. Aleksenko, B.K. Keppler, Chem. Rev. 106 (2006) 2224−2248.

[29] V. Pichler, J. Mayr, P. Heffeter, O. Dömötör, É.A. Enyedy, G. Hermann, D. Groza, G. Kollensperger, M. Galanksi, W. Berger, B.K. Keppler, C.R. Kowol, Chem. Commun. 49 (2013) 2249−2251.

[30] Y. Zhang, A. Ho, J. Yue, L. Kong, Z. Zhou, X. Wu, F. Yang, H. Liang, Eur. J. Med. Chem. 86 (2014) 449−455.

[31] C. Santini, M. Pellei, V. Gandin, M. Porchia, F. Tisato, C. Marzano, Chem. Rev. 114 (2014) 815–862.

[32] N. Shahabadi, M.M. Khodaei, S. Kashanian, F. Kheirdoosh, S.M. Filli, Mol. Biol. Rep. 41 (2014) 3271–3278.

[33] S. Tabassum, M. Zaki, M. Ahmad, M. Afzal, S. Srivastav, S. Srikrishna, F. Arjmand, E. J. Med. Chem. 83 (2014) 141–154.

[34] X.B. Fu, D.D. Liu, Y. Lin, W. Hu, Z.W. Mao, X.Y. Le, Dalton Trans. 43 (2014) 8721–8737.

[35] D. Sanna, P. Buglyó, A.I. Tomaz, J.C. Pessoa, S. Borović, G. Micera, E. Garribba, Dalton Trans. 41 (2012) 12824–12838.

[36] X.-B. Fu, G.-T. Weng, D.-D. Liu, X.-Y. Le, J. Photoch. Photobio. A 276 (2014) 83–95.

[37] F. Tisato, C. Marzano, M. Porchia, M. Pellei, C. Santini, Med. Res. Rev. 30 (2010) 708–749.

[38] K.D. Karlin, Z. Tyeklar, Bioinorganic Chemistry of Copper, Chapman & Hill: New York, 1993.

[39] W. Kaim, J. Rall, Angew. Chem. Int. Ed. 35 (1996) 43–60.

[40] I. Papazoglou, P.J. Cox, A.G. Hatzidimitriou, C. Kokotidou, T. Choli-Papadopoulou, P. Aslanidis, Eur. J. Med. Chem. 78 (2014) 383–391.

[41] C. Belle, C. Beguin, I. Gautier-Luneau, S. Hamman, C. Philouze, J. L. Pierre, F. Thomas, S. Torelli, Inorg. Chem. 41 (2002) 479−491.

[42] E.K. Van den Beuken, B.L. Feringa, Tetrahedron 54 (1998) 12985−13011.

[43] C.J. Cairns, D.H. Busch, Coordin. Chem. Rev. 69 (1986) 1−55.

[44] P. Akilan, M. Thirumavalavan, M. Kandaswamy, Polyhedron 22 (2003) 1407−1413.

[45] L.K. Thompson, F.L. Lee, E.J. Gabe, Inorg. Chem. 27 (1988) 39−46.

[46] A.A. Aruffo, T.B. Murphy, D.K. Johnson, N.J. Rose, V. Schomaker, Inorg. Chim. Acta 67 (1982) L25–L27.

[47] M.F. Iskander, T.E. Khalil, R. Werner, W. Haase, I. Svoboda, H. Fuess, Polyhedron 19 (2000) 949–958.

[48] A. Lyubchova, A. Cosse-Barbi, J.P. Doucet, F. Robert, J.-P. Souron, M. Quarton, Acta Crystallogr. C 51 (1995) 1893–1895.

[49] G.M. Sheldrick. SHELXTL V5.1 Software Reference Manual, Bruker AXS, Inc., Madison, WI, USA (1997).

[50] M.W. Schmidt, K.K. Baldridge, J.A. Boatz, S.T. Elbert, M.S. Gordon, J.H. Jensen, S. Koseki, N. Matsunaga, K.A. Nguyen, S.J. Su, T.L. Windus, M. Dupuis, J. Montgomery, J. Comput. Chem. 14 (1993) 1347–1363.

[51] A.D. Becke, J. Chem. Phys. 98 (1993) 5648–5652.

[52] C. Lee, W. Yang, R.G. Parr, Phys. Rev. B 37 (1988) 785–789.

[53] N.M. O'Boyle, A.L. Tenderholt, K.M. Langner, J. Comput. Chem. 29 (2008) 839–845.

[54] E.D. Glendening, A.E. Reed, J.E. Carpenter, F. Weinhold, NBO (version 3.1)

[55] T. Lu, F. Chen, J. Comput. Chem. 33 (2012) 580–592.

[56] J. Carmichael, W. Degraff, A. Gazdar, J. Minna, J. Mitchell, Cancer Res. 47 (1987) 936–942.

[57] J.A. Marchal, H. Boulaiz, I. Suárez, E. Saniger, J. Campos, E. Carrillo, J. Prados, M.A. Gallo, A. Espinosa, A. Aránega, Invest. New Drug. 22 (2004) 379–389.

[58] J. Yuan, D.B. Lovejoy, D.R. Richardson, Blood 104 (2004) 1450–1458.

[59] X.J. Duan, R.X. Gao, P. Xie, T. Cohen-Karni, Q. Qing, H.S. Choe, B.Z. Tian, X.C. Jiang, C.M. Lieber, Nature Nanotechnol. 7 (2012) 174–179.

[60] E.L. Gelamo, C.H.T.P. Silva, H. Imasato, M. Tabak, Biochim. Biophys. Acta 1594 (2002) 84–99.

[61] J.R. Lakowicz, G. Weber, Biochemistry 12 (1973) 4161–4170.

[62] P.D. Ross, S. Subramanian, Biochemistry 20 (1981) 3096–3102.

[63] G.M. Morris, R. Huey, W. Lindstrom, M.F. Sanner, R.K. Belew, D.S. Goodsell, A.J. Olson, J. Comput. Chem. 30 (2009) 2785–2791.

[64] A. Pal, B. Biswas, S.K. Mondal, C.-H. Lin, R. Ghosh, Polyhedron 31 (2012) 671–675.

[65] M.L. Główka, D. Martynowski, K. Kozłowska, J. Mol. Struct. 474 (1999) 81–89.

[66] T. Steiner, Angew. Chem. Int. Ed. 41 (2002) 48–76.

[67] E. Espinosa, E. Molins, C. Lecomte, Chem. Phys. Lett. 285 (1998) 170−173.

[68] E. Neumann, E. Frei, D. Funk, M.D. Becker, H.H. Schrenk, U. Müller-Ladner, C. Fiehn, Expert Opin. Drug Del. 7 (2010) 915–925.

[69] F. Kratz, T. Roth, I. Fichiner, P. Schumacher, H.H. Fiebig, C. Unger, J. Drug Target. 8 (2000) 305–318.

[70] V.T. Chuang, U. Kragh-Hansen, M. Otagiri, Pharm. Res. 19 (2002) 569–577.

[71] B. Elsadek, F. Kratz, J. Control. Release 157 (2012) 4–28.

[72] T.P.A. Devasagayam, J.C. Tilak, K.K. Boloor, K.S. Sane, S.S. Ghaskadbi, R.D. Lele, J. Assoc. Phys. India 52 (2004) 794–804.

[73] W. Droge, Physiol. Rev. 82 (2002) 47–95.

[74] K. Irani, Y. Xia, J.L. Zweier, J.S. Steven, J.D. Channing, R.F. Eric, S. Maitrayee, F. Toren, J.G.-C. Pascal, Science 275 (1997) 1649–1652.

[75] S.C. Gupta, D. Hevia, S. Patchva, B. Park, W. Koh, B.B. Aggarwal, Antioxid. Redox Sign. 16 (2012) 1295–1322.

[76] M.B. Hampton, S. Orrenius, FEBS Lett. 414 (1997) 552–556.

[77] A. Shrivastava, P.M. Kuzontkoski, J.E. Groopman, A. Prasad, Mol. Cancer Ther. 10 (2011) 1161–1172.

[78] D.B. Lovejoy, P.J. Jansson, U.T. Brunk, J. Wong, P. Ponka, D.R. Richardson, Cancer Res. 71 (2011) 5871−5880.

Figure legends

Scheme 1. Synthesis of copper(II) compounds.

Fig. 1. Crystallography of **C3**: (A) The local coordination environment of **C3**. Hydrogen atoms are omitted. Symmetry code: i = 1 − *x*, − *y*, 2 – z; (B) The N–H···Br interactions in the compound **C3** (Symmetry code: ii = −1 + x, y, z; iii = − *x*, − *y*, 2 − *z*); (C) Perspective view of $\pi\cdots\pi$ interactions in **C3**; (D) Schematic representation of the 4-connected sql topological net of **C3**.

Fig. 2. The molecular graph of **C3** with C–H···O intramolecular H-bonds, the positions of atoms are given, the bond critical points (tiny orange spheres) and the ring critical point (tiny yellow spheres) are also shown.

Fig. 3. Representative dot plots of PI and annexinV double staining on the HepG2 cells in the presence of a 0.25 μM concentration of **C3** and HSA–**C3** for 12 h.

Fig. 4. Cell cycle contributions resulting from treatment with **C3** (0.25, 0.5 and 1.0 μM) for 24 h.

Fig. 5. Intracellular production of reactive oxygen species by **C1**–**C3** and their HSA complexes (0.25 μM) following 48 h incubation. This was determined by flow cytotometric quantification of the fluorescent DCF probe in HepG2 cells: (A), (B) and (C) control cells or cells incubated with **C1**–**C3** and their HSA complexes for 48 h at 37 °C; (D) quantification of the flow cytometric results in (A), (B) and (C) showing the percentage of cells with increased intracellular DCF oxidation compared to control cells. Results are the mean ± SD (n = 5): (**) $p < 0.01$.

Fig. 6. Uv-vis spectra of the PBS buffer of **C1**−**C3** (0.2 mM) after incubation with HSA, with subsequent centrifugation (4000*g*, 10 min).

Fig. 7. (A) Fluorescence quenching spectra of HSA by different concentrations of **C3**. (B) Stern-Volmer plot for the binding of **C1**−**C3** with HSA. (C) Double-log plots for the fluorescence quenching of the HSA by **C1**−**C3**. [HSA] = 1 μM; T = 298 K; pH = 7.4; λex = 280 nm.

Fig. 8. Docking studies of **C1**−**C3** and HSA using Autodock: (A) the overall structure of HSA complex; (B) **C1**−**C3** located within the hydrophobic pocket in subdomain IIA of HSA; (C) The interaction mode between **C1**− **C3** (showing stick representation) and HSA (cartoon form).

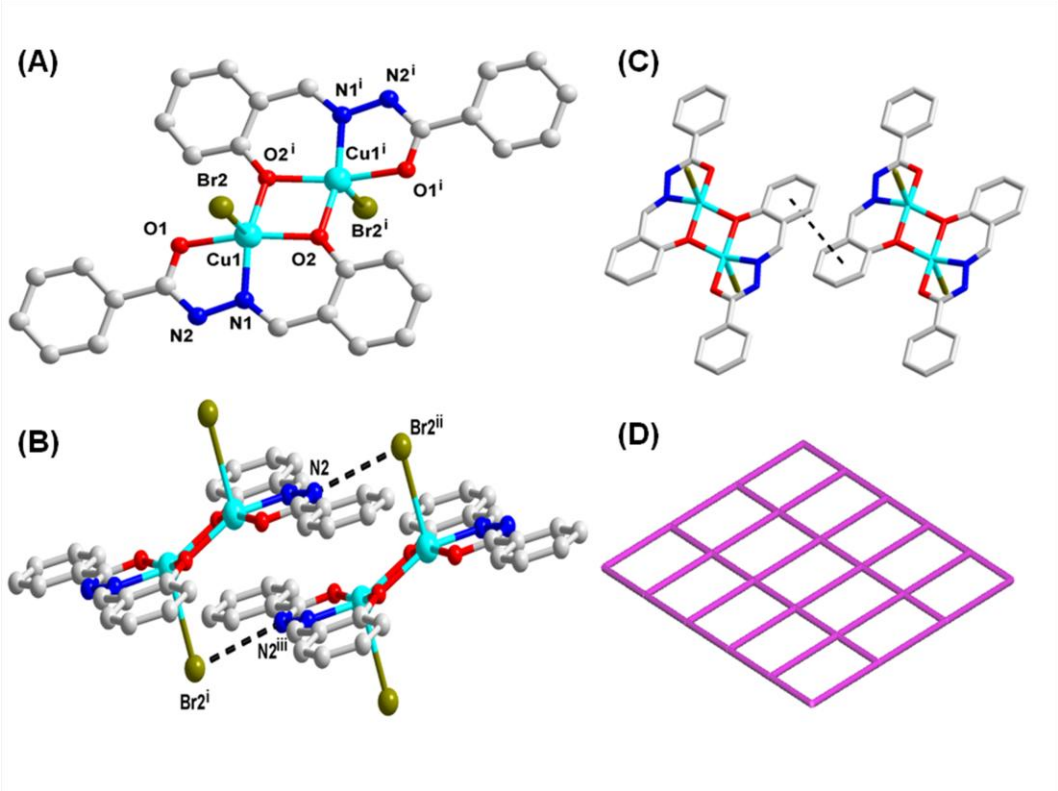

Figure 1

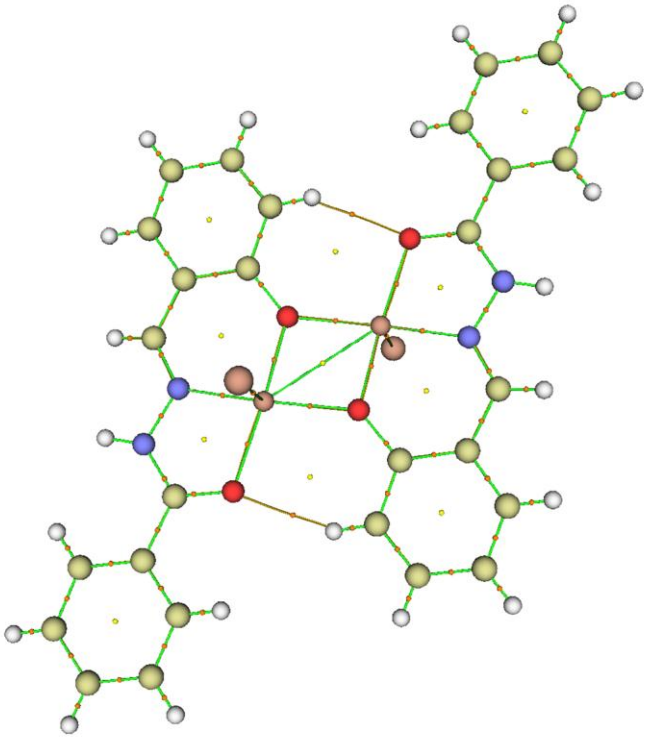

Figure 2

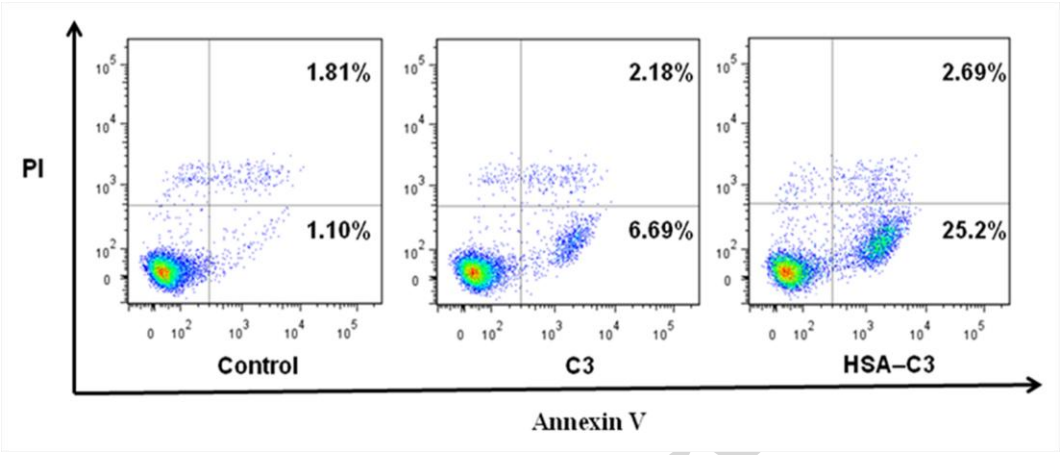

Figure 3

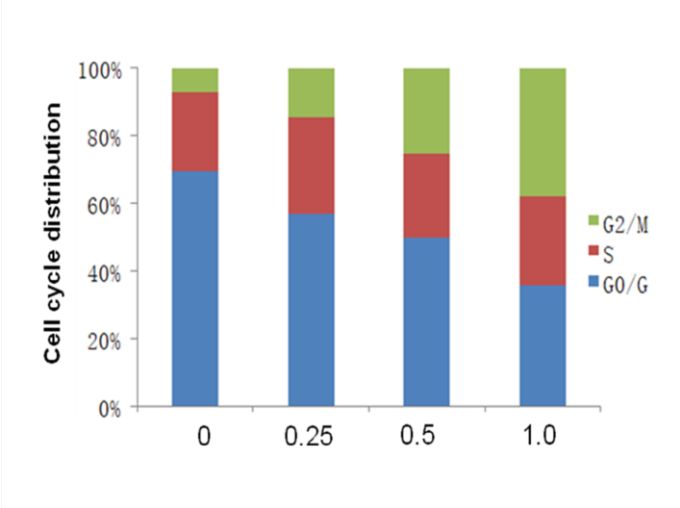

Figure 4

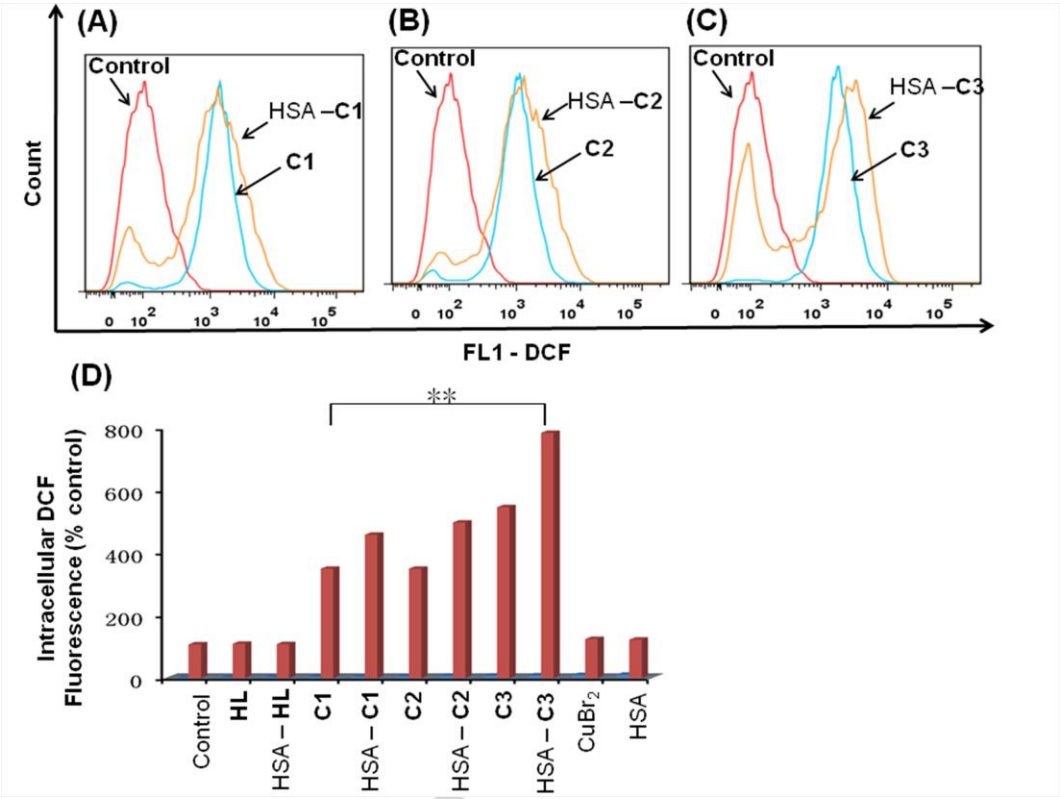

Figure 5

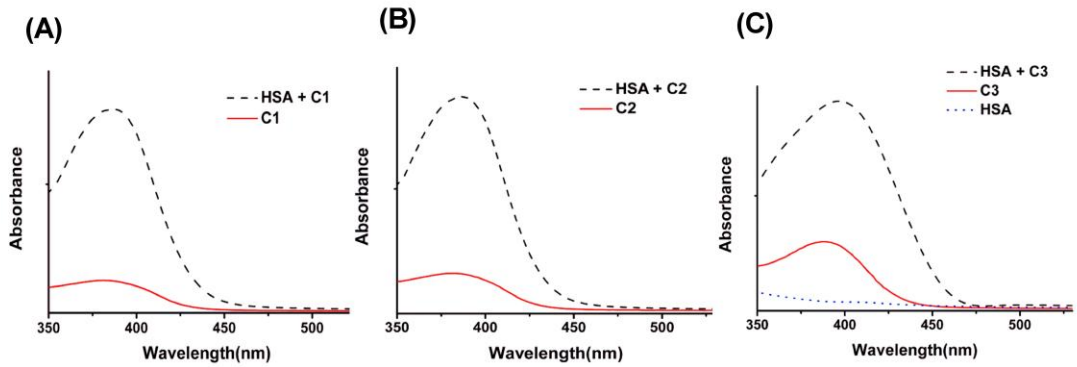

Figure 6

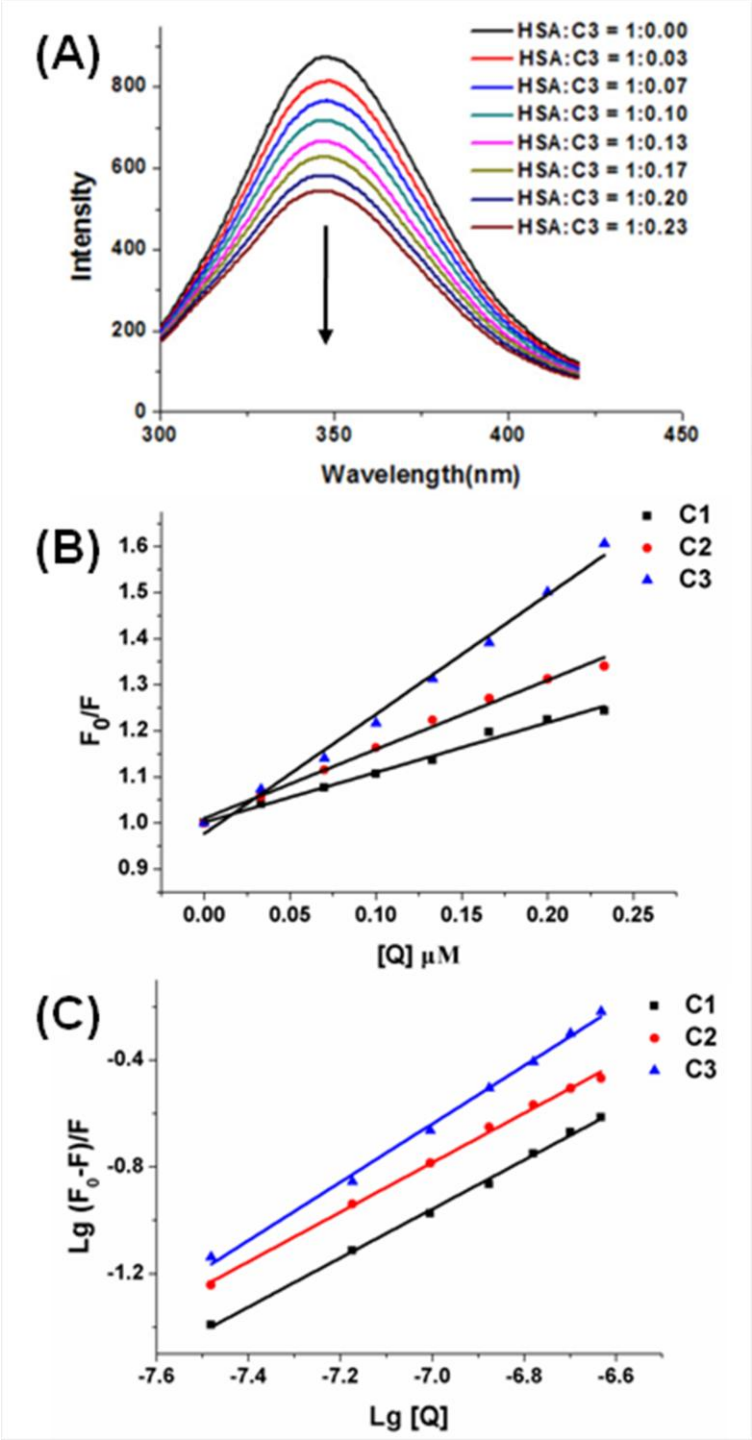

Figure 7

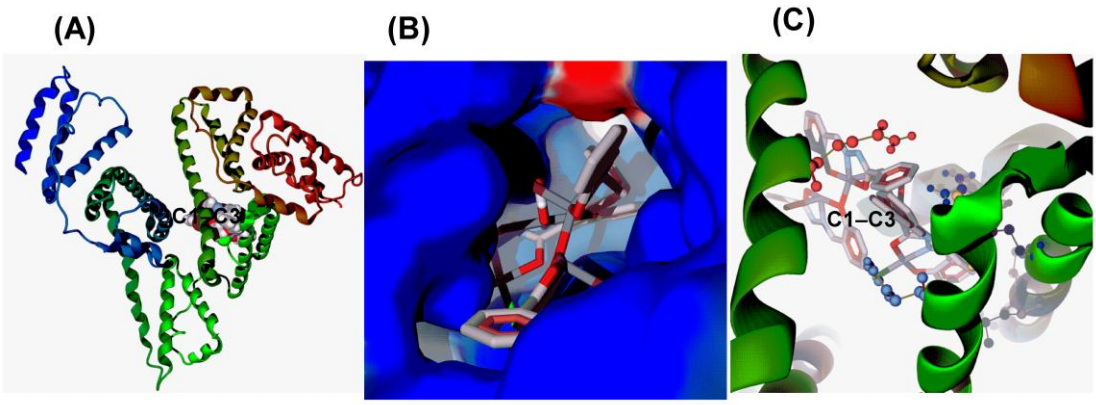

Figure 8

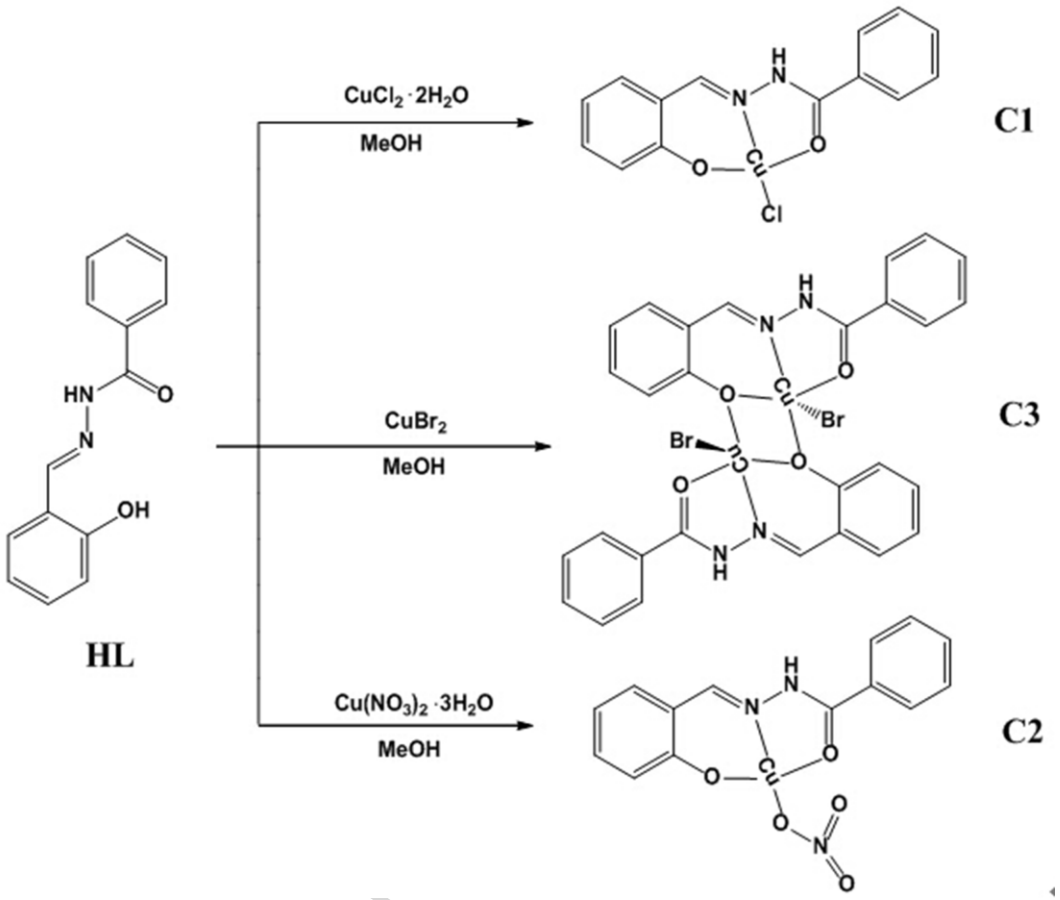

Scheme 1

Table 1 Crystal data for compound **C3**

Complex	**C3**
Empirical formula	$C_{28}H_{22}Br_2Cu_2N_4O_4$
Molecular weight	765.40
Crystal system	triclinic
Space group	*P*-1
a (Å)	6.5655(6)
b (Å)	8.9146(11)
c (Å)	12.0226(15)
α (°)	87.826(10)
β (°)	89.761(9)
γ (°)	79.900(9)
T (K)	291(2)
V (Å^3)	692.26(14)
Z	1
$\rho_{calc.}$ (g·cm^{-3})	1.836
F(000)	378
μ(Mo-K$_\alpha$) (mm^{-1})	4.464
Data/restraint/parameters	2809/2/187
Goodness-of-fit on F^2	0.997
Final R_1, wR_2 [$I > 2\sigma(I)$]	0.0604, 0.1292

Table 2 Selected bond lengths [Å] and angles [º] in compound **C3**

C3			
Cu1–O1	1.967(4)	N1–Cu1–O2	90.8(2)
Cu1–O2	1.939(4)	N1–Cu1–O1	81.0(2)
Cu1–Br2	2.6531(12)	O1–Cu1–O2	164.5(2)
Cu1–N1	1.936(6)	$O2^{i}$–Cu1–O2	79.2(2)
Cu1–$O2^{i}$	1.989(4)	N1–Cu1–$O2^{i}$	157.5(2)
N1–C8	1.288(8)	O1–Cu1–$O2^{i}$	103.60(19)
O2–Cu1–Br2	101.09(14)	N1–Cu1–Br2	97.99(15)
$O2^{i}$–Cu1–Br2	103.73(14)	O1–Cu1–Br2	93.05(14)

Table 3 Topological analysis of **C3**

	ρ_{BCP}/a.u.	$\nabla^2\rho_{BCP}$/a.u.	G_{BCP}/a.u.	V_{BCP}/a.u.	H_{BCP}/a.u.	ε
Cu1–O1	0.080	0.463	0.118	-0.121	-0.003	0.033
Cu1–O2	0.085	0.498	0.127	-0.130	-0.003	0.025
Cu1–N1	0.099	0.495	0.139	-0.155	-0.016	0.026
Cu1–Br2	0.041	0.083	0.031	-0.041	-0.010	0.032
Cu1–O2^{i}	0.074	0.424	0.108	-0.109	-0.002	0.043
C8=N1	0.360	-0.393	0.518	-0.393	-0.113	0.162
C13–H13···O1^{i}	0.013	0.051	0.011	-0.010	0.001	0.076
Ring critical points						
Cu1–O2 –Cu1^{i}–O2^{i}		0.123	0.027			

Table 4. IC_{50} (μM) values of **HL**，**C1**−**C3** and their HSA complexes to different cell lines for 48 h.

compound	Antitumor activity IC_{50} (μM)			
	HeLa	A549	HepG2	HL-7702
HL	>40	>40	>40	>40
HL–HSA	>40	>40	>40	>40
HSA	>100	>100	>100	>100
Cu(II)	>100	>100	>100	>100
Cu(II)–HSA	>100	>100	>100	>100
C1	3.78 ± 0.36	3.75 ± 0.11	2.74 ± 0.22	2.32 ± 0.16
HSA –**C1**	1.42 ± 0.19	2.54 ± 0.24	1.55 ± 0.17	4.75 ± 0.48
C2	3.31 ± 0.26	3.74 ± 0.18	2.92 ± 0.35	2.13 ± 0.23
HSA –**C2**	1.31 ± 0.09	2.08 ± 0.21	1.38 ± 0.16	3.91 ± 0.28
C3	0.84 ± 0.08	1.29 ± 0.07	0.57 ± 0.05	1.24 ± 0.13
HSA–**C3**	0.48 ± 0.07	0.71 ± 0.08	0.25 ± 0.09	1.27 ± 0.11
*Cis*platin	25.52 ± 1.61	17.31 ± 0.72	22.57 ± 1.34	9.19 ± 0.75
HSA–*Cis*platin	>40	>40	>40	37.96 ± 1.21

Table 5 Effects of **C3** and HSA–**C3** on the cell cycle progression in HepG2 cells

compound	Cell cycle		
	G0/G1	S	G2/M
Control	69.41 ± 1.92	23.56 ± 0.28	7.04 ± 0.87
C3	50.83 ± 1.04	27.75 ± 0.54	15.42 ± 0.08
C3–HSA	44.37 ± 0.39	26.94 ± 0.16	28.69 ± 1.10

Table 6 Binding parameters and thermodynamic parameters of HSA complexes

	T(K)	$K_0 \times 10^{-5}$	n	ΔH (kJ·mol^{-1})	ΔG (kJ·mol^{-1})	ΔS (J·mol^{-1}K^{-1})
	298	0.41 ± 0.04	0.89		–26.35 ± 0.04	
C1	310	0.28 ± 0.05	1.03	–22.86 ± 0.04	–26.47 ± 0.04	11.64 ± 0.04
	320	0.22 ± 0.02	1.04		–26.58 ± 0.04	
	298	1.51 ± 0.05	0.91		–29.38 ± 0.04	
C2	310	1.01 ± 0.03	0.99	–27.44 ± 0.03	–29.45 ± 0.03	6.48 ± 0.03
	320	0.69 ± 0.06	0.90		–29.51 ± 0.03	
	298	7.94 ± 0.07	1.01		–33.59 ± 0.03	
C3	310	4.61 ± 0.03	0.99	–29.11 ± 0.03	–33.74 ± 0.03	14.96 ± 0.03
	320	3.56 ± 0.04	0.95		–33.89 ± 0.03	

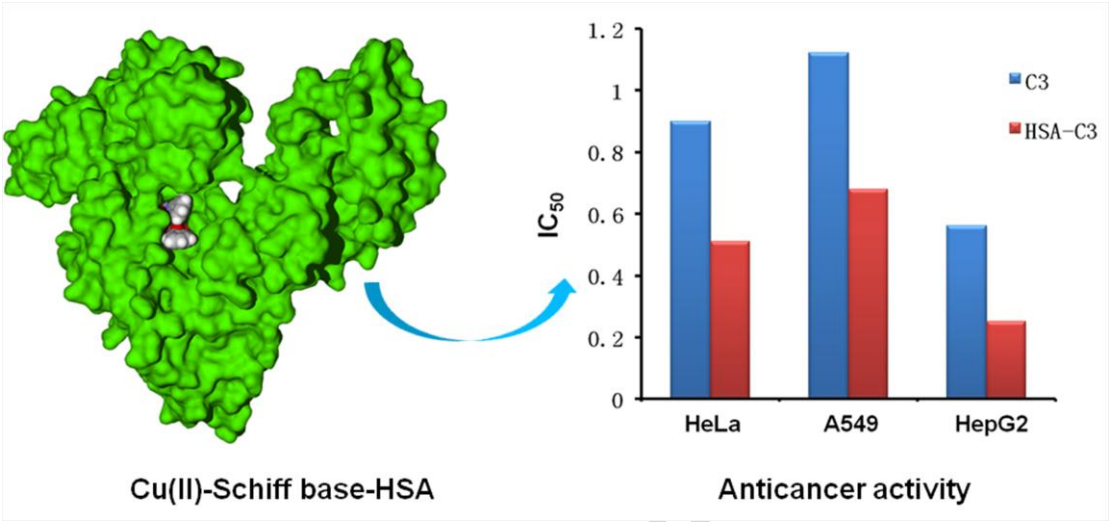

Graphical abstract

Graphical abstract Synopsis

Anticancer activities of copper complexes are improved through bound to IIA sub-domain of HSA.

Highlights

- Novel binuclear Cu(II)-Schiff base complexes were synthesized and characterized.
- The Cu complexes bind to IIA sub-domain of HSA.
- Anticancer activity of the Cu complexes are improved through bound to HSA.